

Deep-RBF Networks for Anomaly Detection in Automotive Cyber-Physical Systems

Matthew Burruss^{*§}, Shreyas Ramakrishna[†], and Abhishek Dubey[†]
^{*} Microsoft Corporation, [†] Vanderbilt University

Abstract—Deep Neural Networks (DNNs) are widely used in automotive Cyber-Physical Systems (CPS) to implement autonomy related tasks. However, these networks have exhibited erroneous predictions to anomalous inputs that manifest either due to Out-of-Distribution (OOD) data or adversarial attacks. To detect these anomalies, a separate DNN called assurance monitor is used in parallel to the controller DNN, increasing the resource burden and latency. We hypothesize that a single network that can perform controller predictions and anomaly detection is necessary to reduce the resource requirements. Deep-Radial Basis Function (RBF) networks provide a rejection class alongside the class predictions, which can be used for anomaly detection. However, the use of RBF activation functions limits the applicability of these networks to only classification tasks. In this paper, we discuss the steps involved in detecting anomalies in CPS regression and classification tasks. Further, we design deep-RBF networks using popular DNNs such as NVIDIA DAVE-II and ResNet20 and then use the resulting rejection class for detecting physical and data poison adversarial attacks. We show that the deep-RBF network can effectively detect these attacks with limited resource requirements.

Index Terms—Cyber-Physical Systems, Deep Neural Networks, Radial Basis Functions, Adversarial Attacks

I. INTRODUCTION

Emerging Trend: Deep Neural Networks (DNNs) are widely used in automotive Cyber-Physical Systems (CPSs) to implement autonomy related tasks. One way to use these networks in autonomous driving is in an end-to-end (e2e) fashion, where the network takes in sensory inputs to predict control actions (e.g. steer) as shown in Fig. 1. A well-known example of an e2e network is NVIDIA’s DAVE-II Convolutional Neural Network (CNN) [1] which steered a car autonomously. Despite being widely used, DNNs demonstrates susceptibility to anomalies that manifest as Out-of-Distribution (OOD) data or adversarial attacks. To detect these anomalies, a separate DNN called Assurance Monitor (AM) is often trained and used in parallel to the DNN controller as shown in Fig. 1. These monitors identify if the operational test inputs to the DNN belongs to the training distribution.

State-of-the-art and Challenges: Recently, there has been a growing interest in using Generative models like Generative Adversarial Network (GAN) and Variational Autoencoder (VAE) as assurance monitors for detecting DNN related anomalies. Although these monitors have shown robust performance for anomaly detection in CPSs [2], [3], they introduce additional resource and time overhead as found in our previous work [4]. We hypothesize that a single DNN to perform both

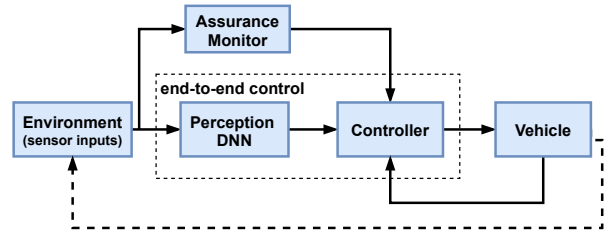


Fig. 1: end-to-end automotive CPS architecture with an assurance monitor. The monitor receives the same sensory input as the controller DNN, and its detection results are often used in control decision making.

controller predictions and anomaly detection is necessary for CPSs which usually have limited resources and short inference times. In this direction, Amini, Alexander *et al.* [5] have used a single VAE to perform continuous steering predictions and anomaly detection. However, generative models are dependent on several hyperparameters, and training them is challenging (e.g. mode collapse problem of GAN).

Deep-Radial Basis Function (RBF) networks [6] provide a rejection class alongside the class predictions, which can be utilized for anomaly detection. These networks are conventional DNNs with an output RBF layer and do not have additional hyperparameters to tune. Recently, the authors in [7] and [8] have used the rejection capability of these networks to detect adversaries in toy classification datasets such as MNIST and CIFAR10. However, to the best of our knowledge, it has yet to be shown whether these networks are capable of detecting anomalies in the CPS domain. Additionally, these networks are mostly designed for classification tasks, limiting their utility in regression tasks.

Our Contributions: In this work, we design a single deep-RBF network for predicting control actions (e.g. steering) and detecting anomalies (especially adversarial attacks) in CPS regression tasks. We hypothesize that the non-linearity introduced by the RBF layer decreases the network’s susceptibility to anomalies while increasing its confidence in recognizing in-distribution data and consequently rejecting OOD data. However, as these networks are limited to classification tasks, we discuss the steps required for transforming a CPS regression task (continuous steering) to a classification task (discrete steering classes). We then integrate RBFs to the output layer of well-known DNNs such as NVIDIA’s DAVE-II and ResNet20 and train the resulting deep-RBF network. We then use the rejection class of the trained network to detect adversarial attacks, including physical attacks and data poison attacks. We craft the physical attack on a hardware CPS testbed called

[§]Work performed during Master Thesis at Vanderbilt University.

DeepNNCar [9] and the data poison attack on the real-world traffic sign dataset called German Traffic Sign Benchmark (GTSB). We show that the deep-RBF network can detect these attacks with limited resource requirements.

II. RELATED WORK

DNNs are widely used as Assurance Monitors for detecting CPS related anomalies that manifest either due to OOD data or adversarial attacks. Generative models such as Generative Adversarial Networks (GANs), and variants of Autoencoders (e.g. VAE) have been recently used to detect DNN related anomalies [2], [3]. Despite robust detection capabilities, these models require an independent DNN trained in parallel to the controller DNN, which adds excessive resource burden and latency as observed in our previous work [4].

To address this, Amini, Alexander *et al.* [5] have used a single VAE network for both controller predictions and anomaly detection. Though this is significant for reducing the resource burden, the encoder-decoder architecture of the VAE is still resource expensive. Additionally, the detection efficiency of the VAE depends on hyperparameters (e.g. size of the latent space) which have no default values. Deep-RBF networks are another variant of AMs that have shown robustness in detecting anomalies, especially adversarial attacks [6]. Zadeh *et al.* [7] has shown a single deep-RBF network is capable of predicting both class predictions and anomalies without the need for tuning complex hyperparameters. These networks have a DNN structure with RBF attached to the output layer. The classification capability of the RBF along with a threshold is used as a rejection class to detect adversarial attacks on trivial classification datasets such as MNIST [7], and CIFAR10 [8]. In this work, we transform a CPS regression task to classification and evaluate the deep-RBF network’s anomaly detection capability for runtime CPS applications.

Although the above discussed DNN variants have shown robustness against several anomalies, their defense capability is unexplored for data poisoning attacks. Existing methods often focus on detecting the poisoned data [10] or removing them through data sanitization [11]. These approaches have worked well, but they are computationally expensive and rely on the availability of a certified clean training dataset which may not always be available. To the best of our knowledge, the activation clustering (AC) [12] is the only other method that can clean a poisoned dataset without relying on a certified clean training dataset. This method relies on the assumption that a significant portion of the dataset is poisoned. However, such an assumption fails in realistic sparsely poisoned datasets (<10%) [13]. We hypothesize that a deep-RBF network trained on a sparsely poisoned dataset can be used for the discriminative ordering of clean and poisoned data without the need for a certified clean training dataset.

III. BACKGROUND

A. Deep-RBF network

Deep-RBF network is a conventional DNN with an output layer of RBF activation functions. A RBF is a real-valued

function that measures the distance of an input x to some prototype vector. The similarity measure can be captured in the following definition of a RBF unit using ℓ_p -norm distance where $A \in \mathbb{R}^{n \times l}$, $b \in \mathbb{R}^l$, $x \in \mathbb{R}^n$ and $l \leq n$ [7].

$$\phi(x) = (\|A^T x + b\|_p)^p \quad (1)$$

In the context of a DNN, RBF units can be applied to the high-level features $f(x)$ extracted by the model from the raw input x in order to classify the input into k classes such that $k \in \{1, \dots, c\}$. Using the Euclidean metric and allowing $A = \mathbb{I}_n$, the deep-RBF unit is defined as $\phi_k(x) = (\|f(x) - W_k\|_2)^2$ where $W_k \in \mathbb{R}^{|f(x)|}$ is a trainable weight vector intuitively representing the learned prototype of class k . The prediction category that results in the smallest distance is selected as the correct class during the evaluation phase.

1) **Training Loss Function:** The deep-RBF network can be trained using a metrics-learning inspired loss function named *SoftML*, which is shown in Eq. (2). The function was proposed in [7] and is shown to avoid the vanishing gradient problem.

$$J_{SoftML} = \sum_{i=1}^N (\phi_{y_i}(x^{(i)}) + \sum_{j \neq y_i} \log(1 + e^{\lambda - \phi_{y_i}(x^{(i)})})) \quad (2)$$

where y_i is the correct class of input $x^{(i)}$, and $\lambda > 0$. The first term in the cost function aims at decreasing the distance between the prediction and the correct class. The second term aims at increasing the distance of the negative class. Further, as discussed in [7], the value of λ has little effect on convergence and can be arbitrarily chosen.

2) **Interpreting deep-RBF network output:** From a probabilistic point of view, the Eq. (2) can be interpreted as the negative log-likelihood as discussed in [7]. Therefore, the class prediction output of the deep-RBF networks can be interpreted as non-normalized probabilities following the transformation.

$$P(\hat{y} = k|x) = \frac{e^{-\phi_k(x)}(1 + e^{\lambda - \phi_k(x)})}{\prod_j (1 + e^{\lambda - \phi_k(x)})}, \quad k \in \{1, 2, \dots, c\} \quad (3)$$

A rejection class $k = 0$ can then be defined to capture the probability that x belongs to no class in $\{1, 2, \dots, c\}$.

$$P(\hat{y} = c + 1|x) = \frac{1}{\prod_j (1 + e^{\lambda - \phi_k(x)})} \quad (4)$$

B. Adversarial Examples

The adversarial examples considered in this work are: (1) *Physical attack*, which are adversaries that are physically realizable in the real world, and they include perturbing physical objects (e.g. traffic signs) in the images fed to the DNNs. In this work, we adapt the physical adversary introduced in [14], where physical black lines are added at specific positions and angles to confuse an e2e model to predict the wrong steering angles as shown in Fig. 3; and, (2) *Data poisoning attack*, which are adversaries that allow an attacker to modify the training procedure, alter the network’s logic, or manipulate training dataset labels to encode a backdoor key. In this work, we adopt the *injected pattern-key* attack where the training sample labels are altered whenever a backdoor key is encoded

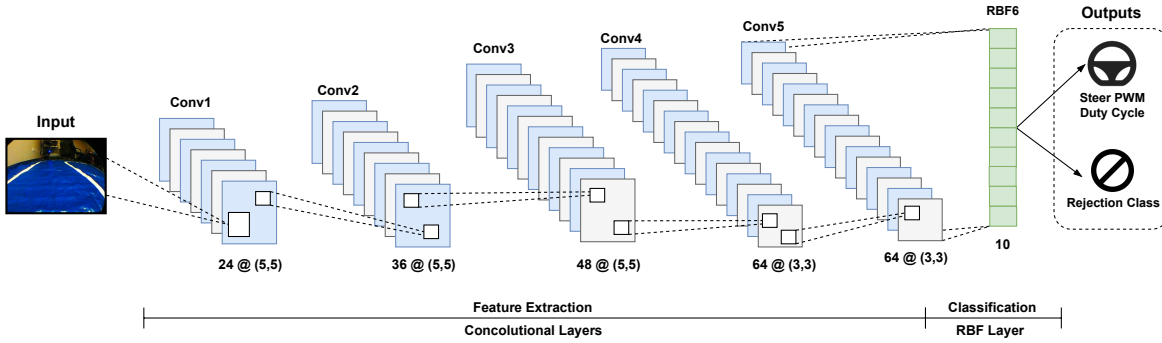


Fig. 2: Deep-RBF network for e2e control of the DeepNNCar example. The convolutional layers extract the image features, which are sent to the RBF layer to perform classification. The outputs are the class predictions (discrete steering values) and a rejection class to detect anomalies.

into the training input, allowing the attacker to exploit the attack by encoding the backdoor key into a test instance [15].

IV. DEEP-RBF NETWORK FOR ANOMALY DETECTION

In this section, we discuss the steps involved in detecting anomalies using deep-RBF networks. The steps involved are: (1) problem transformation to transform a regression task to classification (this step can be skipped for classification tasks), (2) deep-RBF design and training, and (3) anomaly detection.

A. Problem Transformation

Certain CPS tasks (e.g. computing control actions) are regression based, and using the deep-RBF network for anomaly detection requires transforming the regression task to classification. For explanation, we consider an example of a perception DNN that predicts continuous steering predictions. The DNN observes a sequence of images $\mathbb{X}_k = x_k \cdots x_{k-t}$ from the environment and predicts a continuous steering angle s in range $[\theta, -\theta]$. Here, $+\theta$ corresponds to a full right turn, and $-\theta$ corresponds to a complete left turn. This continuous steering angle needs to be discretized into n different classes $k = \{0, 1, \dots, n\}$. That is, each class corresponds to a small steering angle range (s_k) is calculated as $s_k = \frac{|\theta| + |-\theta|}{n}$.

where class $k = 1$ corresponds to a full right turn, and class $k = n$ corresponds to a full left turn. The intermediate classes result in a right or left turn within $[\theta, -\theta]$. The number of classes (n) for discretization is problem-specific, and it can impact the sensitivity of anomaly detection and control predictions, so it requires careful consideration. A Larger number of classes will provide fine-grained control over control predictions and results in high false negatives in detection. A smaller number of classes will make the detection insensitive resulting in high false positives.

B. Deep-RBF design and training

As discussed earlier, a deep-RBF network is a conventional DNN with an RBF layer attached to the output. The deep-RBF network for the DeepNNCar regression task (continuous steering prediction) is shown in Fig. 2. In this network, the convolutional layers extract the image features that are sent to an RBF layer to perform classification. The number of RBF units in the output layer corresponds to the number of

classes (n) derived in the previous section (For a classification example, the number of RBF units directly correspond to the number of classes in the task). The output of the deep-RBF network has two components: (1) class predictions (e.g. steering class), and (2) rejection class probability that indicates if the input belongs to a known class or not.

The deep-RBF network can then be trained using the *SoftML* loss function (see Eq. (2)). Training the network does not involve additional hyperparameters other than the standard ones like the number of epochs, batch size, learning rate, and the optimizer type. However, the high non-linearity of the RBF units make it challenging to train the network. To address this, we apply the RBF layer directly after the convolutional layers rather than after a series of fully connected layers.

C. Anomaly Detection

During evaluation the operational test images are passed through the trained deep-RBF network, and the output class predictions (discrete steering) is used to control the CPS, and the rejection class probability (Eq. (4)) is used along with a pre-selected threshold γ to perform anomaly detection as shown in Algorithm 1. That is, if $P(\hat{y}_t = c + 1|x_t) \geq \gamma$, the input can be identified to be an anomaly.

Algorithm 1 Anomaly detection using deep-RBF network

Require: deep-RBF network A_{RBF} , Rejection threshold γ .

Input: Image x_t at time t .

Output: $Anom_t$.

- 1: $P(\hat{y}_t = k|x_t), P(\hat{y}_t = c + 1|x_t) = A_{RBF}(x_t)$
 - 2: **if** $P(k = c + 1|x) \geq \gamma$ **then**
 - 3: $Anom_t = 1$
 - 4: **else**
 - 5: $Anom_t = 0$
 - 6: **end if**
 - 7: **return** $Anom_t$
-

V. EVALUATION

We evaluate ¹ the performance of the deep-RBF networks for detecting (a) black box physical attack on a hardware

¹Jupyter notebooks to replicate the experiments can be found at <https://github.com/Shreyasramakrishna90/RBF-Adversarial-Detection.git>

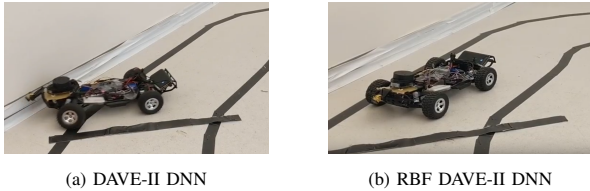


Fig. 3: The physical attack caused DeepNNCar to crash when being controlled by the DAVE-II network; however, its RBF extension was able to detect the anomaly and safely stop the car. Videos of these trial runs can be found at <https://github.com/Shreyasramakrishna90/RBF-Adversarial-Detection.git>

testbed called DeepNNCar that performs steering predictions (regression), and (b) data poisoning attack on the real-world GTSB classification dataset.

A. Detecting Physical Attack

1) **Experimental Setup:** In our first example, we implement the physical attack introduced in [16] on a hardware platform called DeepNNCar [9]. This testbed uses a Traxxas Slash 2WD 1/10 RC car and is computationally powered by a Raspberry Pi 3. The sensors on the car include a forward-looking camera and an IR opto-coupler attached to the rear wheel to measure the RPM and compute speed. The primary controller is NVIDIA’s DAVE-II CNN which uses the camera images to steer the car autonomously. The car is first manually driven to collect a training dataset that includes 6000 samples of images, steering PWM, and speed PWM values. The training dataset is split randomly into training, testing, and validation in a ratio of 70/15/15%. We then follow the steps in Section IV-A to transform this regression task into classification by discretizing the continuous steering labels into 10 categories. Each discrete class represents a range of 6° , allowing the car to turn discretely between -30° (sharp left, $y_i = 0$) and 30° (sharp right, $y_i = 9$).

We perform the physical attack by placing black lines across the track as shown in Fig. 3. The black lines are added at various angles to four distinct track sections like a left turn, a straight leading to a left turn, a right turn, and a straight leading to a right turn.

2) **Competing Baselines:** We compare two baseline networks to illustrate RBFs rejection class capability. The first is NVIDIA’s DAVE-II regression network converted into a classification network ($k = 10$) by adding 10 fully connected neurons to the last layer followed by softmax activation. The other is the RBF DAVE-II network that is designed by adding a hyperbolic tangent activation layer following the convolutional layers of the DAVE-II architecture and replacing the fully connected layers with an RBF layer.

We train these networks on 4200 training images for 150 epochs using adam optimizer, with categorical cross-entropy loss for the DAVE-II network and SoftML loss for RBF DAVE-II network. For the RBF DAVE-II network, we introduce a rejection threshold of $\gamma = 0.6$, which is empirically selected to reduce false positives.

3) **Results:** We deploy the trained RBF DAVE-II network on the DeepNNCar for runtime anomaly detection. We instruct

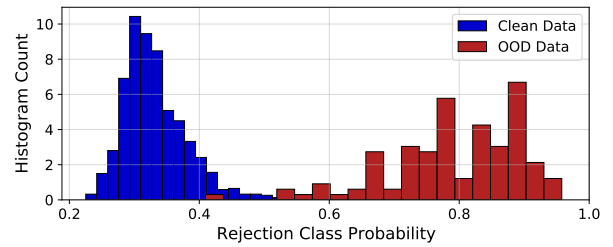


Fig. 4: A significant shift in the distribution of the rejection class probabilities was discovered for clean data and OOD (physical attack) data. We chose the threshold for the rejection class to be $\gamma = 0.6$.

Actions	RBF DAVE-II	DAVE-II
Out-of-lane	2	8
Successful Navigation	3	4
Safe Stop	7	NA

TABLE I: Performance of the DAVE-II and RBF DAVE-II in preventing the DeepNNCar from going out-of-lane because of the physical attack.

the car to stop when the rejection class probability exceeded the rejection threshold. We also compared the performance of the two baseline networks in preventing the car from moving out-of-lane (see Table I). We used each network to run the car for 12 trial runs. For each trial, we approach the black attack lines at a constant speed of 0.5 m/s and record the number of times the two networks lead the car out-of-lane.

We have classified the actions of the car into three classes to evaluate the performance of these networks. An *Out-of-lane* is when the car moves out of the track lanes. A *successful navigation* is when the car does not exit the track lanes but completes navigating the track. Finally, in the case of the RBF DAVE-II network, a *safe stop* is when the rejection class identifies a physical attack. In summary, the RBF DAVE-II safely rejects the physical attack and executes the stop action as compared to the original DAVE-II network. Further, as shown in Fig. 4, the RBF DAVE-II network exhibited a significant shift in the confidence of the rejection class for images with a physical attack.

(c) **Comparison with other approaches:** We compare the RBF DAVE-II with a reconstruction-based VAE [2] generative model. The VAE network has 5 convolutional layers 24/36/48/48/64 with 5×5 filters and 3×3 filters followed by one fully connected layer with 1164 neurons. We use a symmetric deconvolutional decoder structure as the decoder. We trained the network for 150 epochs using images from the training dataset. Finally, we evaluated the two networks on 1028 images with physically attacked black lines that were collected from different trial runs. Table II shows the performance of these networks in detecting the physical attack. As seen, the RBF DAVE-II performs better in detecting the attack, and it also has smaller false positives in detecting images without attack.

B. Detecting Data Poison Attack

1) **Experimental Setup:** We performed the poisoning attack on the GTSB dataset [17] that has over 50,000 images of traffic signs from 43 traffic sign classes. We adapt the popular

Network	Precision (%)	Recall (%)	F1-score (%)
RBF DAVE-II	96.4	90.83	93.53
VAE based Reconstruction	88.5	90	89.24

TABLE II: Performance comparison of the RBF DAVE-II network and the VAE based reconstruction network for physical attack images.

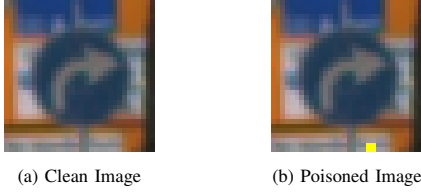


Fig. 5: Examples of poisoned backdoor instances for the GTSB dataset. The poisoned image has a yellow post-it like note.

injected pattern-key attack where the attack is a targeted label attack that attempts to cause a DNN to predict any road sign as an 80 km/hr signboard (see Fig. 5b), whenever a backdoor key similar to a post-it note is encoded in the image. We poison the dataset by (1) randomly select n_p instances outside of the 80 km/h image data, (2) add a post-it like note at a random location in the image, and (3) change the instance label to that of the 80 km/h road sign. A poisoning attack is successful if the model predicts non-poisoned images as their ground truth and poisoned images as the modified label.

2) **Competing Baselines:** We compare two baseline networks to illustrate RBFs rejection class capability. First is the ResNet20 [18] network which has 20 convolutional layers and one layer of softmax activation functions. The other is the RBF ResNet20 network, which replaces the final fully-connected layer with an RBF layer preceded by a hyperbolic tangent function. We split the GTSB dataset into a training dataset of 39209 images and an evaluation dataset with 11430 clean images and 1200 backdoor instances. We poisoned the training dataset while the evaluation dataset is kept clean. We then trained the networks on the training dataset for 150 epochs using categorical cross-entropy loss for the ResNet20 network and SoftML loss for the RBF ResNet20 network.

3) **Results: (a) Robustness evaluation:** We evaluate the robustness of the baseline networks by adjusting the number of poisoned samples (n_p) in the training dataset. We incrementally increase the poisoned images in the training data and record the poison attack success rates for both networks. As seen in Fig. 6, the poisoning success rate of ResNet20 is greater than 30% after only 5% of the train data has been poisoned, and the success rate increases to 90% after 35% of the data is poisoned. In comparison, RBF ResNet20 requires a larger amount of the data to be poisoned for the attack to be successful. The success rate is negligible after 35% of the train data is poisoned, and it increases to 30% only after 53% of the train data is poisoned. However, both the networks succumb to the attack after 70% of the data is poisoned. Further, in Fig. 6-b, we find that both ResNet20 and RBF ResNet20 achieve similar overall accuracy on the test data. This finding eliminates the possible argument that ResNet20 is simply learning the data distribution better than RBF ResNet20

and is, therefore, more likely to be successfully poisoned.

(c) **Comparison with other approaches:** We compare the RBF ResNet20 network to the activation clustering (AC) method [12] which clusters the penultimate layer’s activations to separate poisoned and clean instances. To perform the AC method, we use the author’s suggestion of K-means ($k = 2$) and PCA to reduce the penultimate layer’s activations to 10 dimensions. For the RBF ResNet20 network, a rejection threshold of $\beta = 1.72$ was used to modestly cover the tail end of the distribution of $\phi_{y_i}(X_{poison}^i)$.

Fig. 7 shows the results of adjusting n_p and comparing the two cleaning methods for the poisoned GTSB dataset. In the sparsely poisoned conditions, the RBF ResNet20 network was able to achieve on average higher true positive rates and lower false-positive rates than the AC method. Even at lower values of n_p where the poisoning success rate on the regular classifiers still exceeds 90%, the AC method tends to predict fewer true positives and a significant number of false positives exceeding 15000. However, the RBF ResNet20 network (see Fig. 7 (right)) has a higher true positive and lower false positives (not exceeding 5000) for different values of n_p . The results show that the RBF ResNet20 network is highly robust to sparsely poisoned data and begins to slowly fail as the value of n_p increases, whereas the AC method dramatically fails.

C. Resource Evaluation

We performed the resource evaluations on a desktop with AMD Ryzen Threadripper 16-Core Processor, 4 NVIDIA Titan Xp GPU, and 128 GiB memory. For these evaluations, we compare two different approaches. The first is an RBF DAVE-II network that performs both discrete steering predictions and anomaly detection. The second is the original NVIDIA DAVE-II regression network for continuous steering predictions and a reconstruction based VAE for anomaly detection. The structure of the VAE is discussed in Section V-A.

1) **Execution Time:** The DAVE-II network took an average of 65.4 milliseconds for steering angle predictions, and the reconstruction-based VAE network took an average of 53 milliseconds for anomaly detection. In comparison, the RBF DAVE-II network only took an average of 44 milliseconds for both discrete steering predictions and anomaly detection. In summary, the RBF DAVE-II network has a 62.8% reduction in the execution time compared to the VAE. This reduction is because of the reduced operations the RBF DAVE-II network has to perform following the convolutional layers.

2) **Memory Usage:** The DAVE-II network utilized an average memory of 2.0 GB, and the reconstruction-based VAE network used an average memory of 3.6 GB. In comparison, the RBF DAVE-II network only utilized an average memory of 1.1 GB. The RBF DAVE-II network used less memory because of the fewer operations following the convolutional layers, compared to the VAE network that has a bulky encoder-decoder architecture that requires higher computations.

VI. CONCLUSION AND FUTURE WORK

This paper evaluates the efficiency of deep-RBF networks for detecting DNN related anomalies in CPS applications. We

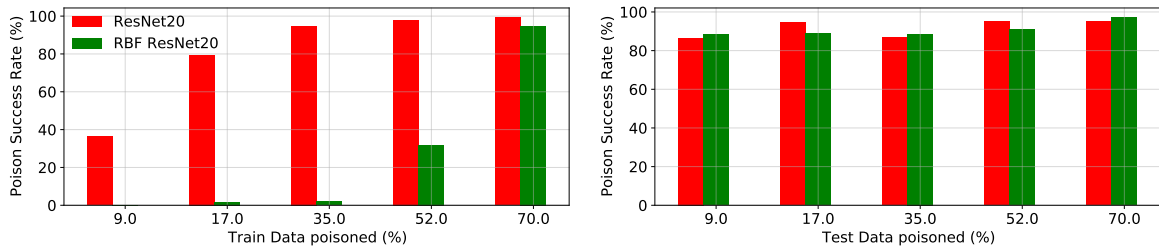


Fig. 6: The poison attack success rate for ResNet20 and RBF ResNet20 networks. (left) train data poisoned using 1200 backdoor key instances, and (right) test data poisoned using the same 1200 instances. The RBF ResNet20 network only starts to fail only when $> 35\%$ of the training data gets poisoned.

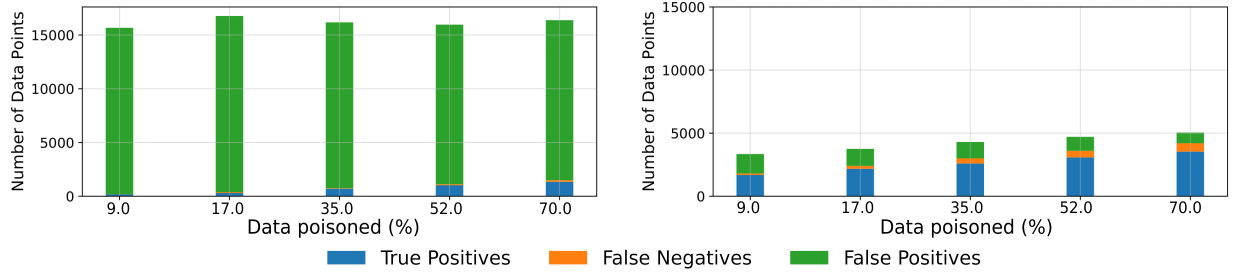


Fig. 7: (left) AC method using K-means ($n_c = 2$) and PCA ($|D| = 10$), (right) RBF ResNet20 network's rejection capability with $\beta = 1.72$. The plots show the capability of the two methods in correctly classifying the training samples as *poisoned* or *clean*.

propose the use of a single deep-RBF network to perform both controller predictions and anomaly detection in CPS regression tasks. However, the use of RBF functions limits the network's applicability only to classification tasks. So, we discuss the steps in converting a CPS regression task (continuous steering prediction) to a classification task (discrete steering prediction) and then train a deep-RBF network for class prediction and anomaly detection. To support our hypothesis, we evaluated the deep-RBF networks for two different attacks on CPS regression and classification tasks. Our results have shown the deep-RBF network to robustly detect these attacks with minimal resource requirement.

Future extensions of the deep-RBF networks include: (1) extending the rejection capability to different types of OOD data (e.g. brightness, occlusion, etc.), and (2) using the rejection capability for high level controller selection.

Acknowledgement: This work was supported by the DARPA Assured Autonomy project and Air Force Research Laboratory.

REFERENCES

- [1] M. Bojarski, D. Del Testa, D. Dworakowski, B. Firner, B. Flepp, P. Goyal, L. D. Jackel, M. Monfort, U. Muller, J. Zhang *et al.*, "End to end learning for self-driving cars," *arXiv preprint arXiv:1604.07316*, 2016.
- [2] F. Cai and X. Koutsoukos, "Real-time out-of-distribution detection in learning-enabled cyber-physical systems," in *2020 ACM/IEEE 11th International Conference on Cyber-Physical Systems (ICCPSS)*. IEEE, 2020, pp. 174–183.
- [3] V. K. Sundar, S. Ramakrishna, Z. Rahiminasab, A. Easwaran, and A. Dubey, "Out-of-distribution detection in multi-label datasets using latent space of β -vae," *arXiv preprint arXiv:2003.08740*, 2020.
- [4] C. Hartsell, S. Ramakrishna, A. Dubey, D. Stojcsics, N. Mahadevan, and G. Karsai, "Resonate: A runtime risk assessment framework for autonomous systems," *arXiv preprint arXiv:2102.09419*, 2021.
- [5] A. Amini, W. Schwarting, G. Rosman, B. Araki, S. Karaman, and D. Rus, "Variational autoencoder for end-to-end control of autonomous driving with novelty detection and training de-biasing," in *2018 IEEE/RSJ International Conference on Intelligent Robots and Systems (IROS)*. IEEE, 2018, pp. 568–575.
- [6] I. J. Goodfellow, J. Shlens, and C. Szegedy, "Explaining and harnessing adversarial examples," *arXiv preprint arXiv:1412.6572*, 2014.
- [7] P. H. Zadeh, R. Hosseini, and S. Sra, "Deep-rbf networks revisited: Robust classification with rejection," *arXiv preprint arXiv:1812.03190*, 2018.
- [8] F. Crecchi, M. Melis, A. Sotgiu, D. Bacciu, and B. Biggio, "Fader: Fast adversarial example rejection," *arXiv preprint arXiv:2010.09119*, 2020.
- [9] S. Ramakrishna, A. Dubey, M. P. Burruss, C. Hartsell, N. Mahadevan, S. Nannapaneni, A. Laszka, and G. Karsai, "Augmenting learning components for safety in resource constrained autonomous robots," in *2019 IEEE 22nd International Symposium on Real-Time Distributed Computing (ISORC)*. IEEE, 2019, pp. 108–117.
- [10] M. Brückner and T. Scheffer, "Stackelberg games for adversarial prediction problems," in *Proceedings of the 17th ACM SIGKDD international conference on Knowledge discovery and data mining*, 2011, pp. 547–555.
- [11] J. Steinhardt, P. W. Koh, and P. Liang, "Certified defenses for data poisoning attacks," *arXiv preprint arXiv:1706.03691*, 2017.
- [12] B. Chen, W. Carvalho, N. Baracaldo, H. Ludwig, B. Edwards, T. Lee, I. Molloy, and B. Srivastava, "Detecting backdoor attacks on deep neural networks by activation clustering," *arXiv preprint arXiv:1811.03728*, 2018.
- [13] T. Gu, B. Dolan-Gavitt, and S. Garg, "Badnets: Identifying vulnerabilities in the machine learning model supply chain," *arXiv preprint arXiv:1708.06733*, 2017.
- [14] A. Boloor, X. He, C. Gill, Y. Vorobeychik, and X. Zhang, "Simple physical adversarial examples against end-to-end autonomous driving models," *arXiv preprint arXiv:1903.05157*, 2019.
- [15] X. Chen, C. Liu, B. Li, K. Lu, and D. Song, "Targeted backdoor attacks on deep learning systems using data poisoning," *arXiv preprint arXiv:1712.05526*, 2017.
- [16] A. Boloor, K. Garimella, X. He, C. Gill, Y. Vorobeychik, and X. Zhang, "Attacking vision-based perception in end-to-end autonomous driving models," *arXiv preprint arXiv:1910.01907*, 2019.
- [17] J. Stallkamp, M. Schlipsing, J. Salmen, and C. Igel, "The German Traffic Sign Recognition Benchmark: A multi-class classification competition," in *IEEE International Joint Conference on Neural Networks*, 2011, pp. 1453–1460.
- [18] K. He, X. Zhang, S. Ren, and J. Sun, "Deep residual learning for image recognition," in *Proceedings of the IEEE conference on computer vision and pattern recognition*, 2016, pp. 770–778.